NKS-445
ISBN 978-87-7893-537-3

# Towards high-fidelity fuel pellet fracture modelling in current and new fuel designs

Janne Heikinheimo[1]

Jussi Peltonen[1]

Diogo Ribeiro Costa[2]

[1]VTT Technical Research Centre of Finland Ltd

[2]KTH Royal Institute of Technology, Sweden

March 2021

## Abstract

Cracking of $UO_2$ clearly requires detailed understanding of local microscopic and macroscopic stresses. Also, the structural details and their effects on the microcracking should be known. To improve the fuel fracture modelling, we have started the work towards binding the structural features of the pellets with the crack behaviour modelling. The report shows measurements of a standard pellet with EBSD techniques and reviews macroscopic stress behaviour in 2D horizontal plane for differently sized pellets applying the BISON fuel performance code.

The SEM-EBSD results of a standard $UO_2$ pellet showed a dense microstructure with small and round pores in inter- and intra-granular locations, which are characteristic of such a fuel. There was no preferential crystallographic orientation in the sample.

The stress behaviour in the fuel pellets was modelled during different power-up ramp rates. The varying diameter of pellets did not show any particular differences in the stress behaviour, except for the maximum stress location due to reduced pellet-cladding gap. Introducing a macroscopic crack in the pellet caused localization of the stress and the smeared cracking model of the BISON code worked well.

## Key words

SEM-EBSD, $UO_2$ structure, BISON fuel performance code, von Mises stress, cracking

NKS-445
ISBN 978-87-7893-537-3
Electronic report, March 2021
NKS Secretariat
P.O. Box 49
DK - 4000 Roskilde, Denmark
Phone +45 4677 4041
www.nks.org
e-mail nks@nks.org

# Towards high-fidelity fuel pellet fracture modelling in current and new fuel designs

## Final Report from the NKS-R POMMI (Contract: AFT/NKS-R(20)131/7)


Janne Heikinheimo[1]
Jussi Peltonen[1]
Diogo Ribeiro Costa[2]

[1]VTT Technical Research Centre of Finland Ltd
[2]KTH Royal Institute of Technology, Sweden

# Table of contents

## 1. Introduction

Fuel pellet deformation is a complex problem including several physical phenomena at different length and time scales. In the OECD/NEA report, four key phenomena have been identified with the ongoing research programs (mainly for LWR applications): creep, swelling, cracking and mechanical deformation in pellet-clad interaction (PCI) (OECD, 2015). Fuel cracking behaviour modelling is important since it directly impacts the fission product release and fuel thermal conductivity.

The parabolic temperature gradient in the fuel pellet causes tensile stresses in the outer regions of the pellet, where the fuel is brittle. The inner parts of the fuel experience compressive stress and with high enough temperature and stress rates the deformation is increasingly plastic (Canon et al., 1971). A macroscopic stress in the fuel can cause diverging local stresses and microcracking due to e.g. strain incompatibilities between the grains (Salvo et al., 2015). Porosity in $UO_2$ also affects strongly to the yield stress and fracture strength of the material (Igata and Domoto, 1973; Radford, 1979). In addition, localization of pores in grains or at grain boundaries, their size and shape have a strong impact on $UO_2$ cracking behaviour (Oguma, 1982; Werner and Routbort, 1983). Recently, mesoscale approaches have been developed for $UO_2$ plastic deformation as well as for brittle fracture to simulate the microstructural evolution and cracking in the fuel (Chakraborty et al., 2016; Portelette et al., 2018).

Cracking of $UO_2$ clearly requires detailed understanding of local microscopic and macroscopic stresses. Also, the structural details and their effects on the microcracking should be known. To improve the fuel fracture modelling, we have started the work towards binding the structural features of the pellets with the crack behaviour modelling. This report summarizes experimental methodology and structural measurements of the standard pellet with electron backscatter diffraction (EBSD) technique and reviews macroscopic stress behaviour in 2D horizontal plane for differently sized pellets applying the BISON fuel performance code.

## 2. Experimental methods

Electron backscatter diffraction (EBSD), which is also known as backscatter Kikuchi diffraction (BKD) or electron backscatter pattern technique (EBSP), is a methodology that analyses backscattered electrons (BSE) that undergo coherent electron diffraction by crystals in the specimen's surface (few nanometres depth). The EBSD system is basically composed of a holder used to tilt the sample 70° to the electron beam, an EBSD BSE detector that contains a phosphor screen to collect the diffracted BSEs over a large solid angle, and a digital camera. This technique is widely used to determine the local crystal structures, the phase fractions, and the crystal orientations with all the associated measurements in different materials (texture, grain size, strain, boundary characterisation, etc.) (Schwartz et al., 2009). For instance, EBSD is used to characterise standard uranium dioxide ($UO_2$) nuclear fuel (Iltis et al., 2015; Maslova et al., 2019; Nerikar et al., 2011; Saada et al., 2019, 2021), as well as advanced fuel concepts such as uranium nitride (UN) (Johnson & Lopes, 2018) and UN-$UO_2$ composites (Costa et al., 2020).

The uranium dioxide ($UO_2$) pellet used in this study was supplied by Westinghouse Electric Sweden AB. The pellet was sintered in a hydrogen atmosphere at 1780 °C for about 4 h, producing a sample with a density of 10.53 g/cm$^3$ or 96.1 % of the $UO_2$ theoretical density (Rundle et al., 1948). Naturally enriched $UF_6$ ($U^{235}$ = 0.71 wt%) was used to fabricate the $UO_2$ fuel at Westinghouse via ammonium uranium carbonate (AUC) wet route (Hälldahl, 1985; Lee et al., 1991).

The sintered $UO_2$ pellet was cut longitudinally at KTH and hot mounted in a phenolic resin with carbon filler for the SEM-EBSD examinations. The mounted sample was ground with SiC paper and polished using diamond suspensions, followed by a final polishing treatment with aluminium oxide suspension (0.05 mm, Buhler Masterprep) to provide a defect-free surface for the EBSD analyses. This last polishing is important since EBSD is a surface technique, which obtains information from a thin layer of the material (few nanometres). A Gatan PECS coater was used to cover the polished sample with a conducting carbon layer (2 nm) for the measurements.

The EBSD analyses were carried out in a high-resolution field emission gun (FEG) scanning electron microscope (SEM) model Zeiss GeminiSEM 450, coupled with an EBSD (Oxford instruments Synergy) and the software AZTEC. Secondary electron (SE) and backscatter electron (BSE) detectors were used to assess the microstructure morphology at 15 kV. Three regions of the $UO_2$ microstructure were examined at different magnifications, i.e. 200X (one region) and 1000X (two regions). Step sizes of 1 µm and 0.15 µm were used during the EBSD mapping acquisitions at 200X (analysed area of 1000 µm x 1000 µm) and 1000X (analysed area of 200 µm x 200 µm), respectively.

From the EBSD results, the inverse pole figure (IPF) maps, Euler angles (EAs), $UO_2$ grain boundaries, and the equivalent circle diameter (µm) distributions were obtained and are reported in this document.

## 3. Stress and cracking modelling with the BISON code

The BISON fuel performance code is being developed at Idaho National Laboratory, and is based on MOOSE (Multiphysics Object-Oriented Simulation Environment) framework (Hales et al., 2016a, 2016b). The BISON code is capable of 1.5D, 2D and 3D fuel rod behaviour analyses. Typically fuel performance codes apply 1.5D approach, where the pellet thermomechanical behaviour is solved only in the radial direction and the axial nodes are bound together by the free volume gas pressure and the coolant boundary conditions. Increasing the number of dimensions increases the computational effort, but can bring details into modelling that are not possible to take accurately into account in 1.5D analysis.

In this work, we have applied a finite element 2D plane approach and studied stress field of an $UO_2$ pellet during power ramps. For the intact pellets the number of radial nodes was 30 and the number of outer circumferential nodes was 60. For the pellet with a macroscopic crack, the number of radial nodes was 15 and the number of outer circumferential nodes was 30.

For the stress analysis we monitored equivalent tensile stress or von Mises stress. The von Mises stress gives a scalar value for the total stress at different material points, and can be used e.g. to confirm if the stress level has reached the material yield strength. The von Mises values can be calculated from the material stress tensor.

The stress in the material depends in general on the temperature difference between different regions of the pellet that causes different thermal expansion. When the stress reaches the material's yield value, plastic deformations in the pellet reduce the stress. In addition, neutron irradiation and accumulated fission products cause creep and stress in the pellet. The creep rate of the fuel caused by irradiation and thermal effects is modelled as

$$\dot{\epsilon} = \frac{A_1 + A_2\dot{F}}{(A_3 + D)G^2}\sigma \cdot exp\left(\frac{-Q_1}{RT}\right) + \frac{A_4}{(A_6 + D)}\sigma^{4.5} \cdot exp\left(\frac{-Q_2}{RT}\right) + A_7\dot{F}\sigma \cdot exp\left(\frac{-Q_3}{RT}\right), \tag{1}$$

where $\sigma$ is the effective (von Mises) stress, $T$ is the temperature, $D$ is the fuel density, $G$ is the grain size, $\dot{F}$ is volumetric fission rate, $Q_i$ are the activation energies, and $R$ is the universal gas constant. The first term of equation (1) models diffusional thermal creep at low temperatures, the second term accounts for the creep due to thermal dislocations and the third term describes the irradiation induced creep (Allison et al., 1993). The fuel structure also changes via fission product accumulation and release. The associated fuel swelling is addressed with the empirical MATPRO correlations (Allison et al., 1993). Fuel densification at the beginning of life is calculated with the ESCORE empirical model (Rashid et al., 2004). We also applied model for fuel (radial) relocation, where cracked fuel fragments change the fuel radial strain. The effective radial relocation strain is calculated according to the modified ESCORE relocation model (Kramman and Freeburn, 1987).

The BISON code has some ready models for material cracking. In this study, we applied a so-called smeared cracking model. The model reduces the stress in the fuel and increases effective fuel volume when cracking occurs. If the principal stress exceeds the critical stress value at certain material point, the material point is considered cracked at that direction and stress at that point reduced to zero. The material point does not have after cracking any strength unless the strain becomes compressive. The numerical solution becomes increasingly difficult if many material points have multiple cracks.

## 4. Results and discussion

### 4.1. Electron backscatter diffraction (EBSD) analyses of a standard uranium dioxide pellet

**Figure *1*** reports the SEM-SE image, as well as the IPF and EA maps from the EBSD taken at 200X in the marked area (1000 µm x 1000 µm). Additionally, the pole figure set and the equivalent circle diameter distribution of the grains are presented. Figure 2 and Figure 3 show the same results obtained at 1000X in two different regions (200 µm x 200 µm).

The SEM-SE images (
**Figure *1***, Figure 2, and Figure 3) portray a dense microstructure with small and rounded pores, which are characteristic of closed porosity at the end of the sintering process (German, 2014). In the IPF map, or conveniently referred to as a colour key for crystal orientation map (COM), the colours for each grain correspond to the crystallographic orientation in the grain parallel to the normal direction (Z0) (stereographic triangle in the inset) (Nerikar et al., 2011). The Euler angles describe the orientation of the crystallographic axes with respect to the reference frame, being generally used to export the EBSD data (Bunge, 2013; Nolze, 2015). As previously reported (Maslova et al, 2019), there is no preferential crystallographic orientation in the $UO_2$ sample, as observed in the EBSD images in the figures (IPF maps, pole figure sets, EA maps).

The grain size distributions (equivalent circle diameter) show the variety of grains sizes present in the sample.

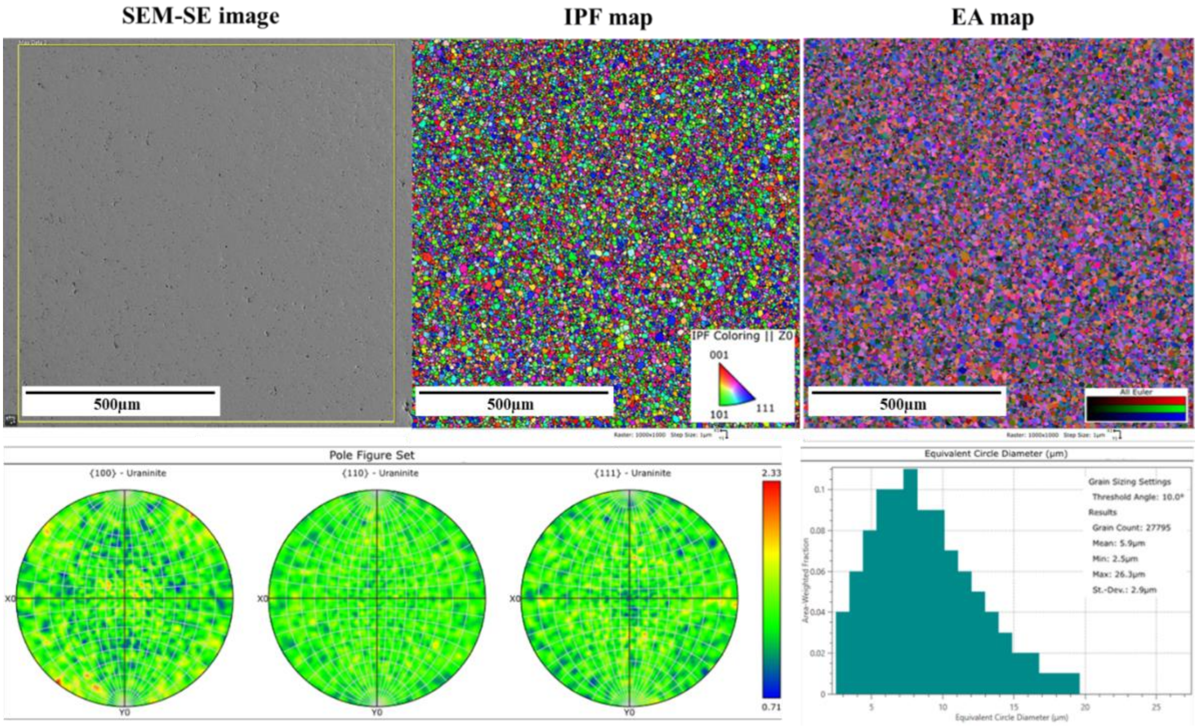


**Figure 1.** SEM-EBSD examinations at 200X of magnification of a standard $UO_2$ fuel showing the microstructure morphology (SEM-SE image), the inverse pole figure (IPF) map in the direction Z0, the Euler angle (EA) map, and the pole figure set and the equivalent circle diameter distribution of the grains. There is no preferential crystallographic orientation in the sample, as shown in the IPF, EA, and pole figure images.

The results obtained at 1000X provided a better view of the grain boundaries (IPF maps). The grains in the $UO_2$ fuel sample were equiaxed in shape and had an average size of about 5 µm. Moreover, small round pores were observed in inter- and intra-granular locations. All these morphological characteristics are in good agreement with previous results for $UO_2$ (Costa et al., 2021; Iltis et al., 2015).

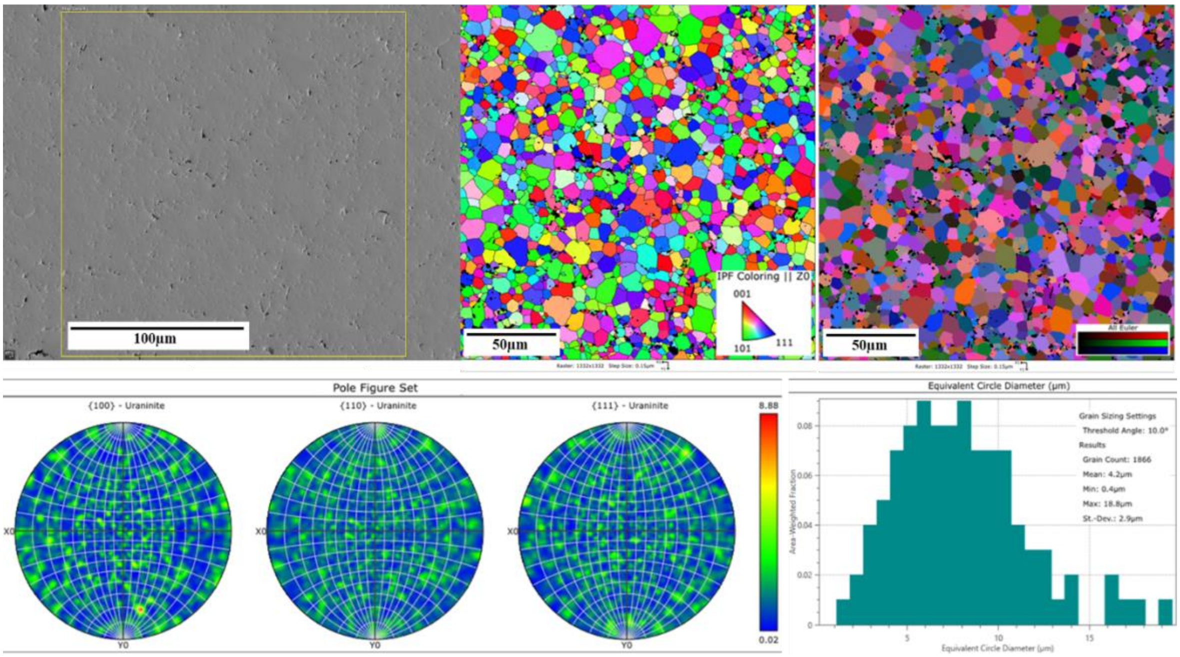


**Figure 2.** SEM-EBSD examinations at 1000X of magnification of a standard $UO_2$ fuel showing the microstructure morphology (SEM-SE image), the inverse pole figure (IPF) map in the direction Z0, the Euler angle (EA) map, and the pole figure set and the equivalent circle diameter distribution of the grains. These images also shown that there is no preferential crystallographic orientation in the sample.

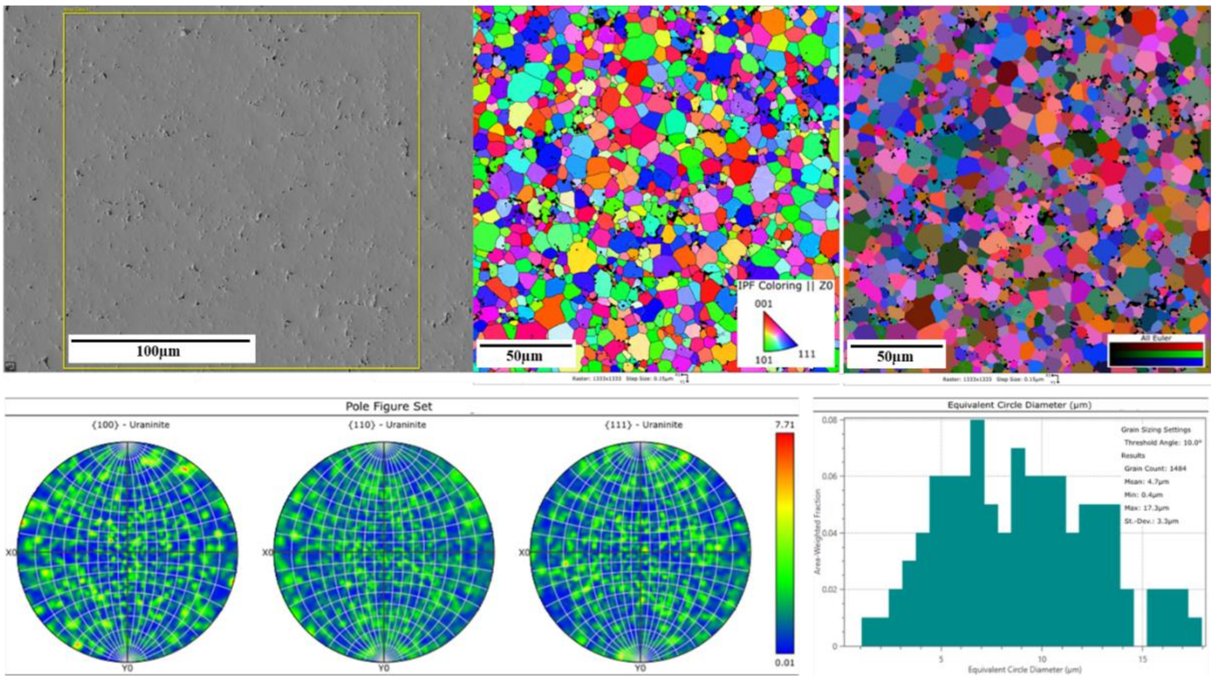


**Figure 3.** SEM-EBSD examinations at 1000X of magnification of a standard $UO_2$ fuel showing the microstructure morphology (SEM-SE image), the inverse pole figure (IPF) map in the direction Z0, the Euler angle (EA) map, and the pole figure set and the equivalent circle diameter distribution of the grains. These images also shown that there is no preferential crystallographic orientation in the sample. The images are taken from a different region of the same sample in comparison to figure 2.

## 4.2. Stress modelling of the $UO_2$ fuel under power ramp conditions

The fuel starts to crack or yield when a specific yield stress exceeds. Pellet fragmentation during nominal loading is mainly characterized by radial and axial cracks (OECD, 2015). The cracks reduce the stress in the fuel and increase the effective volume. To review the general features of stress behaviour of $UO_2$ fuels, we started with the simulations of nuclear fuel pellets by applying a 2D plane approach for quarter pellets, where x- and y-axis boundaries are fixed. With the selected geometry we are able to observe horizontal stress development in the pellet and discuss about the associated fuel radial cracking.

In this section, we study the stress evolution in differently sized pellets and in a pellet with a large macroscopic crack in it. We applied power ramps of 4.5, 9 and 15 kW/m/h for the fresh fuel. The ramp curves are presented in figure 4. For simplicity, we applied abnormally large pellet-cladding gap in the fuel rods (0.2 mm) to avoid pellet-cladding interaction (PCI) in the simulations. For comparison, we kept the power level similar for all fuels. Figure 5 shows the fuel centre line temperature for various pellet diameters in the 9 kW/m/h ramp. The centre line temperature is slightly lower in the larger diameter pellets. One reason for the reduced temperature could be the smaller pellet-cladding gap for the larger diameter fuel as it expands faster. On the other hand, the power (or fission) density is lower in the larger diameter pellets, when the linear power is the same. The cladding of the fuel (Zry-4) had a constant outer surface temperature of 580 K.

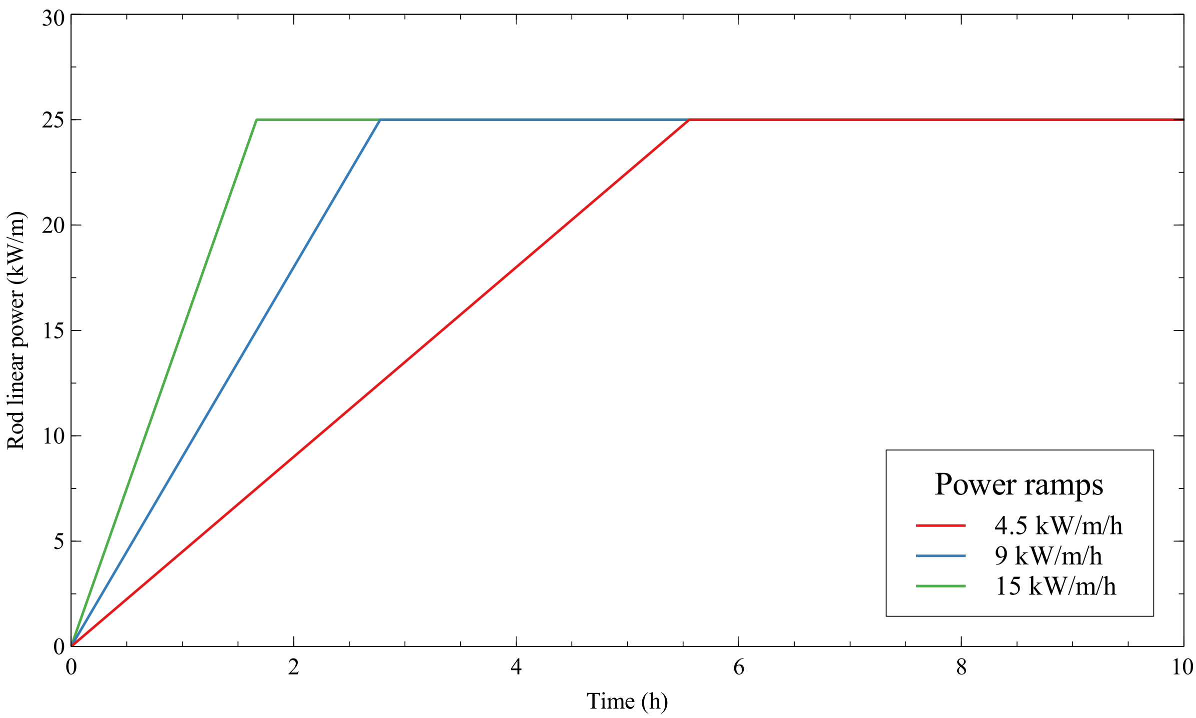


**Figure 4.** Power ramp conditions applied in the simulations.

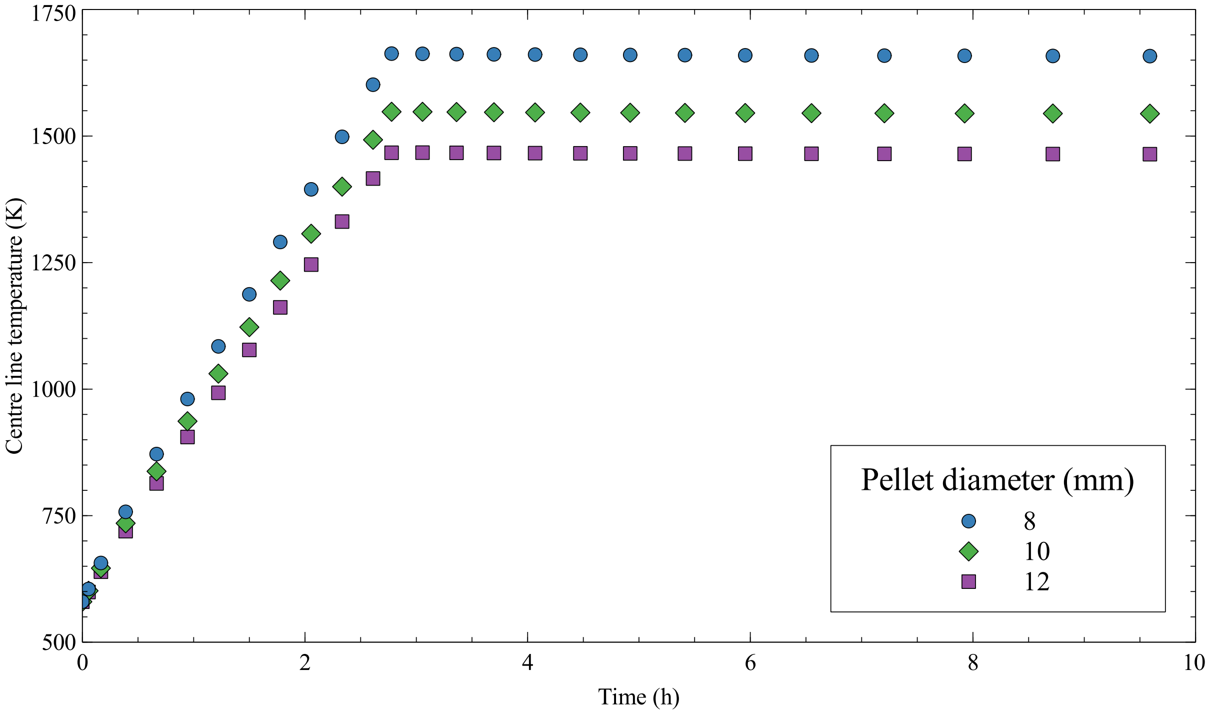


**Figure 5.** Centre line temperature of fuels with different diameters with the 9 kW/m/h ramping.

Figure 6 shows that the maximum von Mises stress of a pellet peaks at the end of a power ramp and reduces with the constant power. It should be noticed that the stress level of a pellet in the 2D model is slightly higher, compared to estimated and calculated realistic stresses in fuel pellets (Hales et al., 2016b; Salvo et al., 2015). In the modelling elastic strain and plastic deformations reduce the stress level. In the present case, we applied plastic deformations due to fuel densification, fission product accumulation and release, thermal and irradiation creep, and radial relocation model (Hales et al., 2016a, 2016b). The radial relocation model calculates effective radial strain due to relocation cracking. Here, we did not apply additional cracking models, that would reduce the stress at the material points. We did not apply fuel plastic deformation due to compressive stresses, which becomes more pronounced at higher temperatures.

The evolution of the stresses in the pellets followed the same pattern with all simulated geometries. First the stress field is strong at the centre of the pellet. Then the stress shifts radially towards the edges of the pellet and gets its maximum value at around 3/4$R$. The stress field continues its journey towards the edges of the pellet at the constant power and reduces slowly. The evolution is illustrated for Ø 8 mm pellet with 9 kW/m/h ramp rate in figures 7-9.

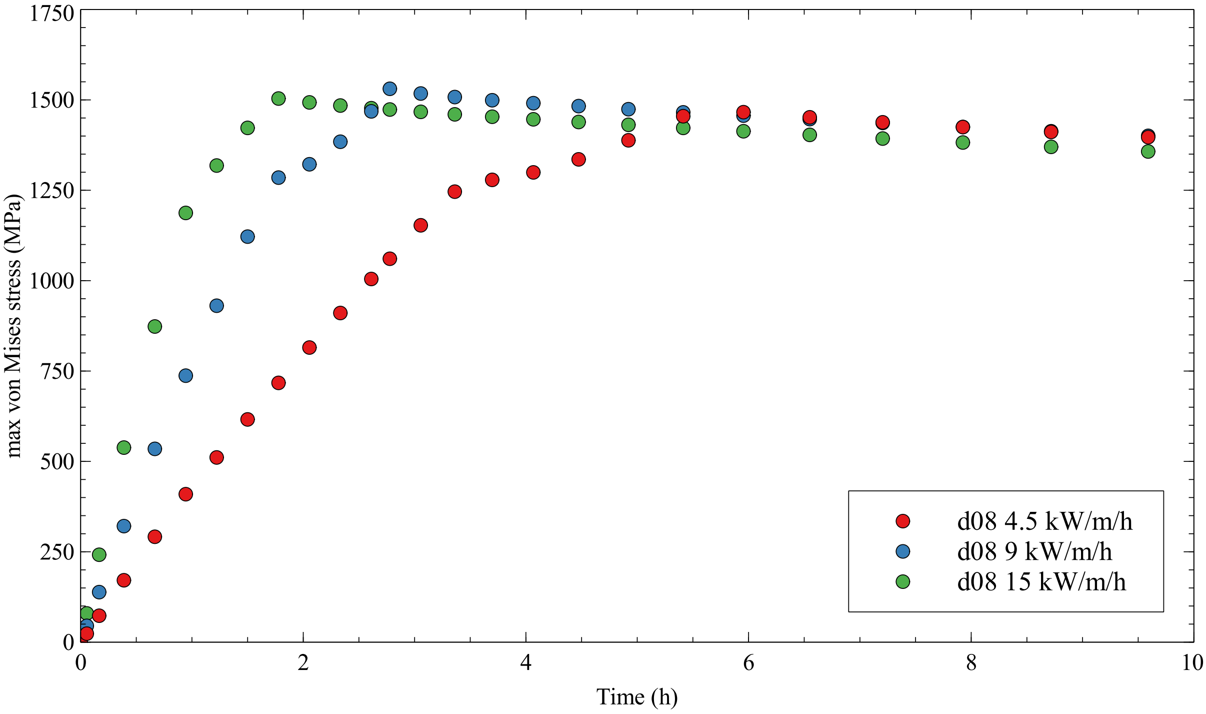


**Figure 6.** Maximum von Mises stress in the Ø 8 mm pellet as a function of time with three different power ramps.

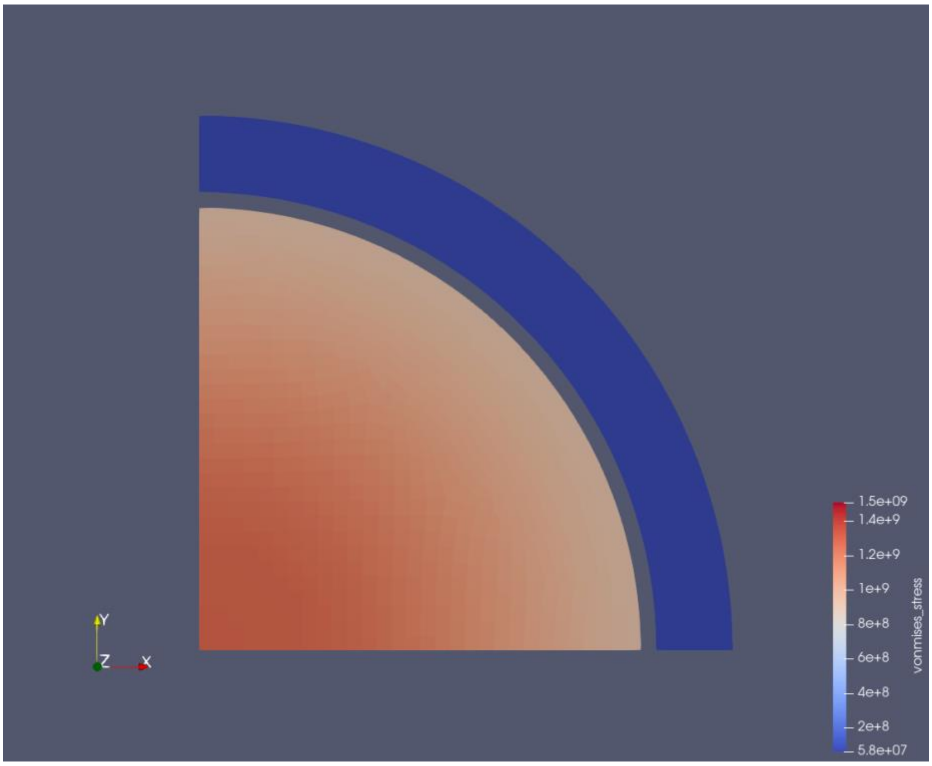


**Figure 7.** von Mises stress in the Ø 8 mm pellet after 1 h 45 min of the 9 kW/m/h ramp start.

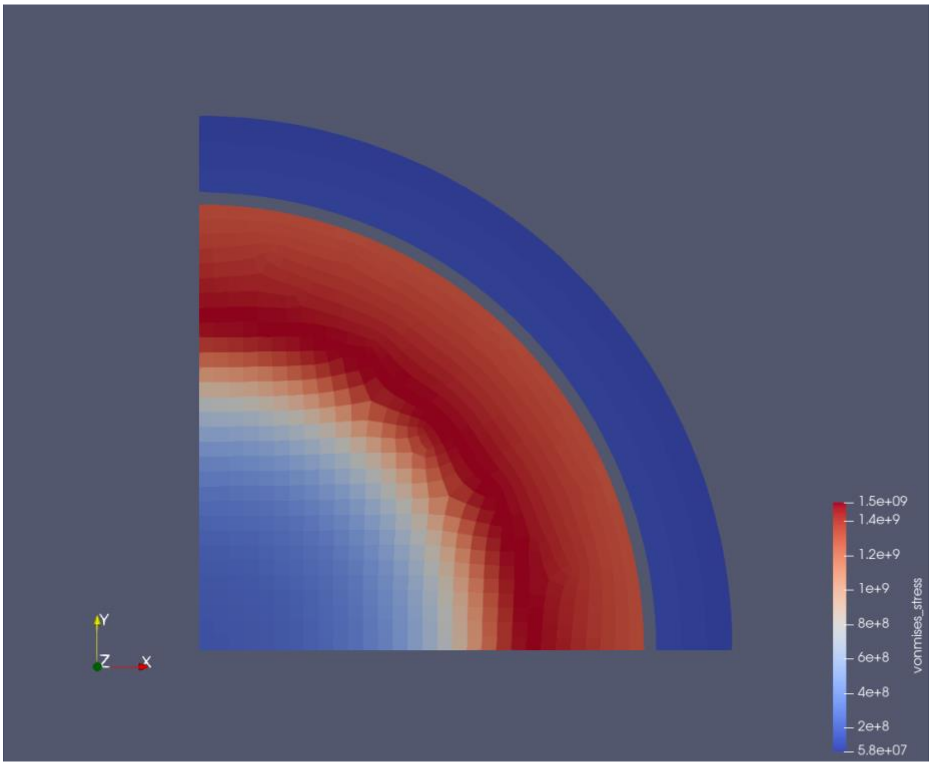


**Figure 8.** von Mises stress in the Ø 8 mm pellet after 2 h 45 min of the 9 kW/m/h ramp start. The stress level reaches its maximum value.

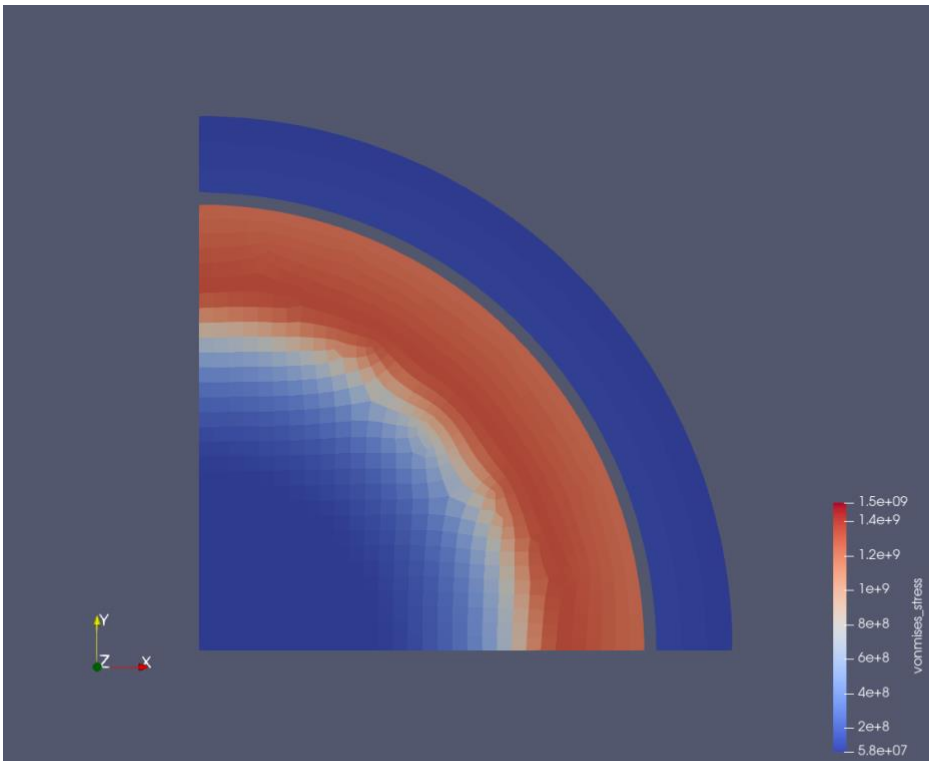


**Figure 9.** von Mises stress in the Ø 8 mm pellet after 11 h 5 min of the 9 kW/m/h ramp start.

While comparing pellets with different diameters, the behaviour (figures 7-9) remained the same. The stress level reached its maximum value right after the ramp in all cases. The stress levels of the simulations are shown in figure 10.

The location of the maximum von Mises stress was relatively closer to the centre of the pellet, when the diameter was increased (figure 11). One of the reasons for the shift is quite probably better gap conductance. The pellet-cladding gap reduces faster in the larger pellets due to their expansion.

The stress and temperature behaviour changes significantly if a macroscopic defect is introduced in the pellet. Figure 12 illustrates the stress of defected pellet at the end of the 9 kW/m/h power ramp. The stress is strongly localized close to the tip of the macroscopic crack.

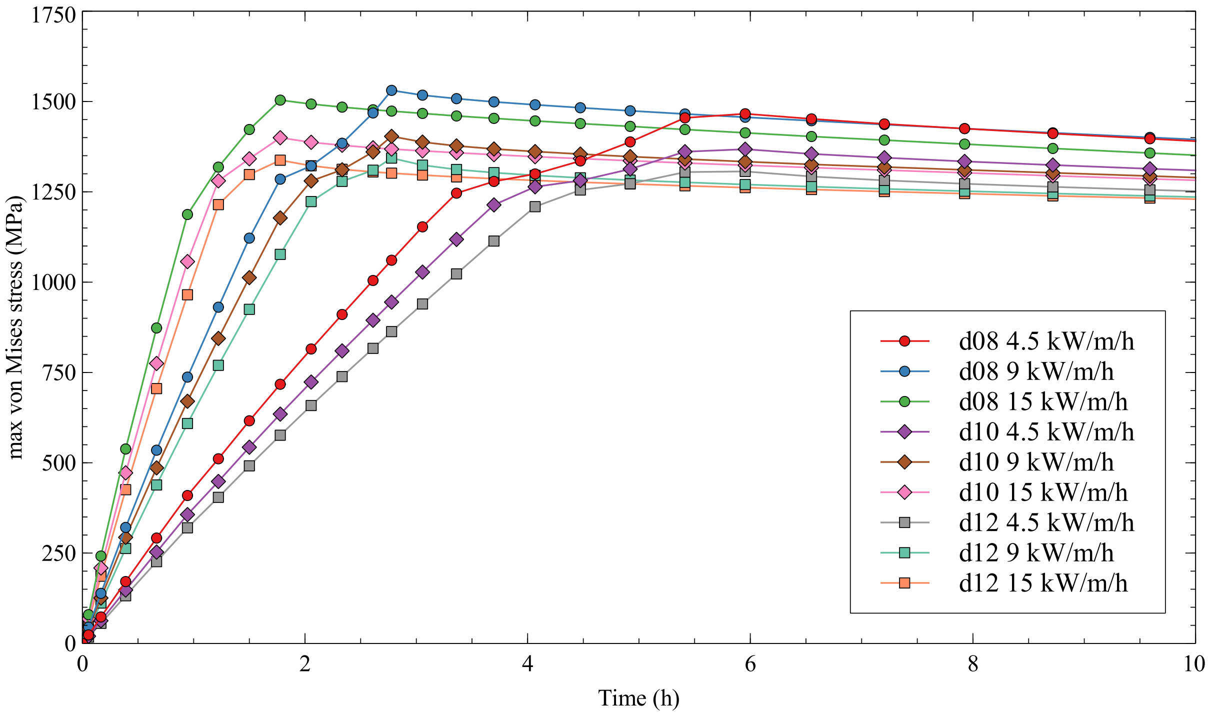


**Figure 10.** Maximum von Mises stress in pellets with different diameters as a function of time with different power ramps.

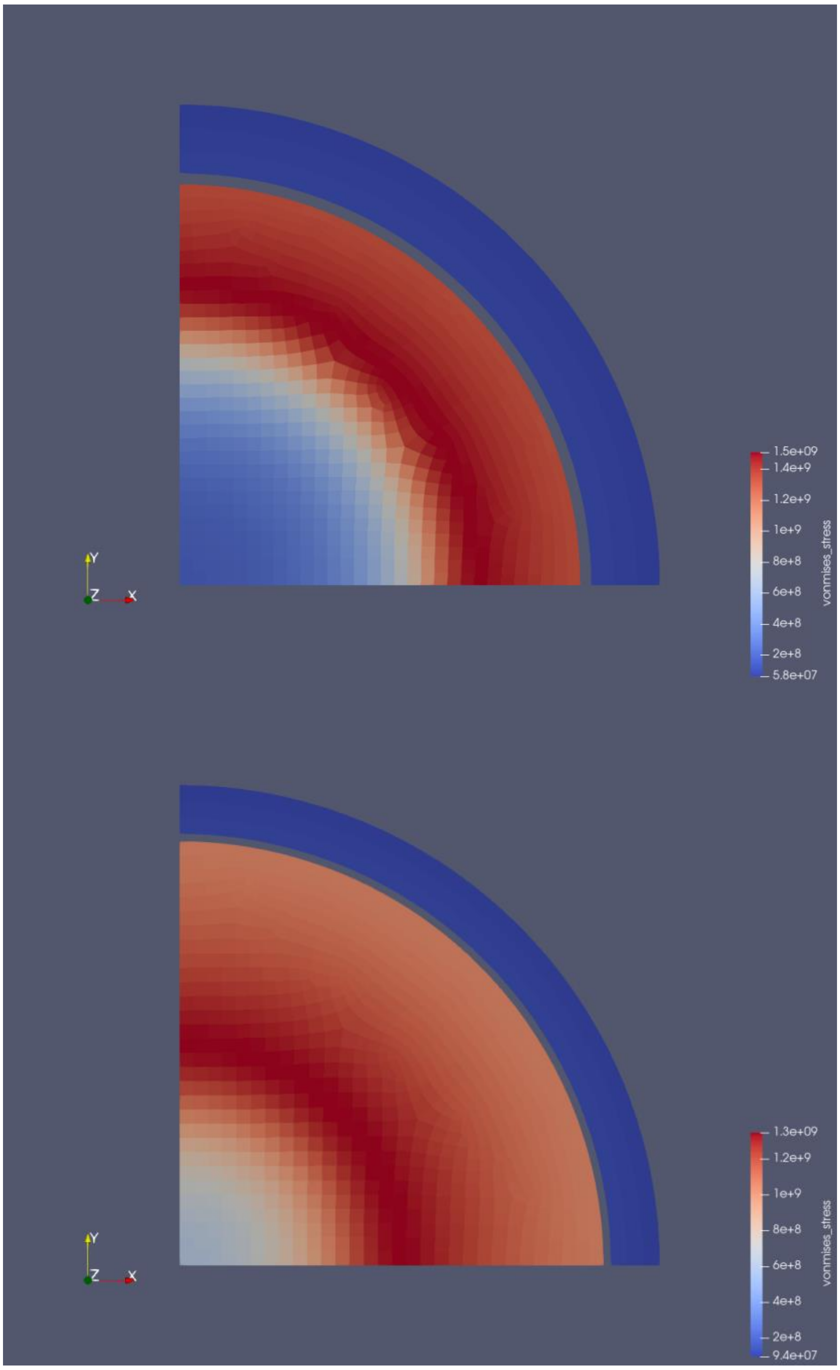


**Figure 11.** Maximum von Mises stress location in Ø 8 mm (upper) and Ø 12 mm (lower) pellets at 2 h 45 min after the 9 kW/m/h ramp start.

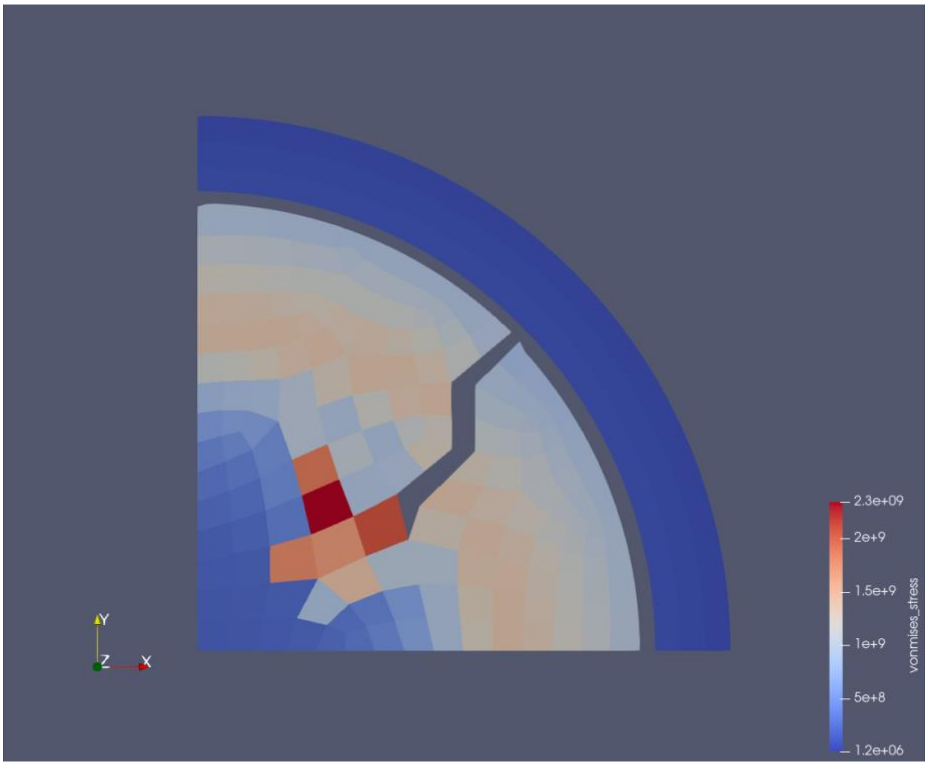


**Figure 12.** von Mises stress in the defected fuel pellet at 2 h 45 min after the 9 kW/m/h ramp start.

### 4.3 Fracture modelling of $UO_2$ fuels

To simulate microcracking in the pellets, a build-in smeared cracking model was added in the modelling. Currently, the model limits to a small number of cells as the computational time increases rapidly. In the first tests, model failed to converge in the case of regularly shaped pellets. Quite probably the evenly distributed von Mises stress complicate the modelling. Fine tuning of the critical stress value could help in reducing the number of cracked cells.

To demonstrate cracking in the defected pellet, we performed simulation to the pellet with a macro crack. The defect helps the modelling as the stress is clearly localized. The microcracks of the defected Ø 8 mm pellet at the end of a 9 kW/m/h ramp are illustrated in figure 13.

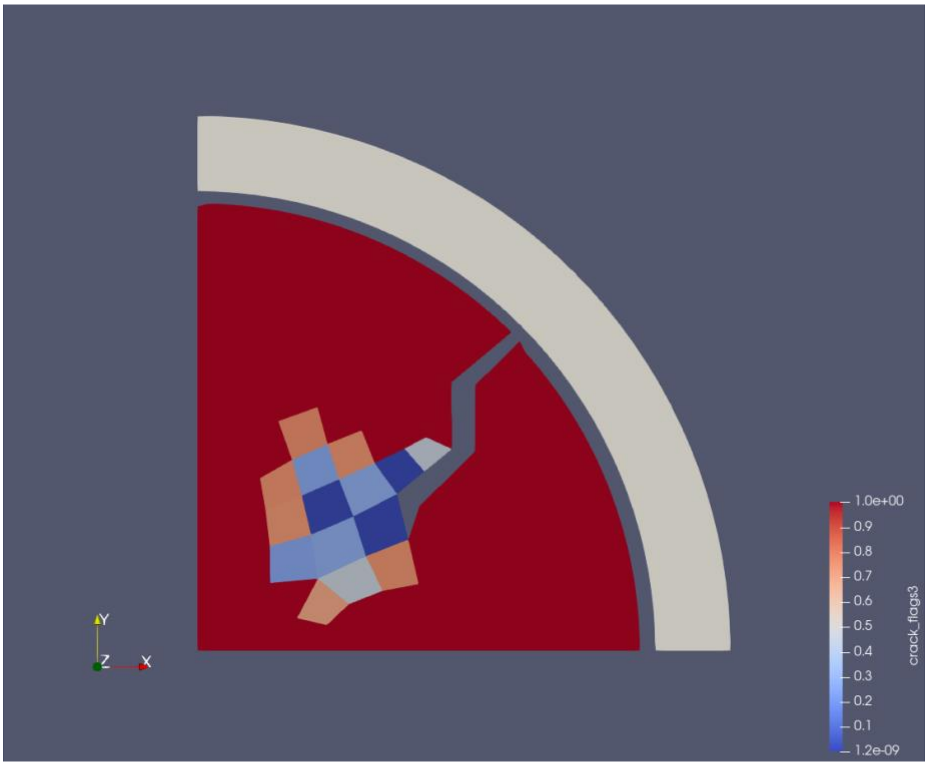


**Figure 13.** Microcrack formation in the Ø 8 mm defected pellet after the 9 kW/m/h ramp. Value 1 indicates that the material point has not cracked and a value below 1 indicates that the cracking has occurred.

## 5. Conclusions

In this work we have measured standard pellet with EBSD techniques and reviewed macroscopic stress behaviour in 2D horizontal plane for differently sized pellets applying the BISON fuel performance code.

The SEM-EBSD results of a standard $UO_2$ pellet showed a dense microstructure with small and round pores in inter- and intra-granular locations, which are characteristic of such a fuel. Additionally, there was no preferential crystallographic orientation in the sample. The grain sizes distributions showed the variety of equiaxed grains present in the specimen, with an average value of about 5 µm.

The stress behaviour in the fuel pellets was modelled during different power-up ramp rates. We applied 4.5, 9 and 15 kW/m/h ramps from 0 to 25 kW/m power. The varying diameter of pellets did not show any particular differences in the stress behaviour, except for the maximum stress location. The reason for the shift is quite probably the reduced pellet-cladding gap at the end of the ramps for larger diameter pellets. The smeared cracking model did not converge in the regularly shaped pellets as the stress was quite evenly distributed. Introducing a macroscopic crack in the pellet caused localization of the stress and the smeared cracking model worked well.

In the future, we plan to implement and develop a crystal-plasticity based approach to describe local deformation phenomena in the fuel pellets. The modelling utilizes the actual microstructure of the pellet based on SEM-EBSD images while the detailed stress fields at different conditions (2D or 3D) can be obtained with dedicated fuel performance codes, such as the BISON code.


## Acknowledgements

This work was funded by NKS (Nordic Nuclear Safety Research), SAFIR2022 (The Finnish Research Programme on Nuclear Power Plant Safety 2019-2022) and KYT2022 (Finnish Research Programme on Nuclear Waste Management 2019-2022).

Diogo Ribeiro Costa is funded by the Swedish Foundation for Strategic Research (SSF, *Stiftelsen för Strategisk Forskning*) through the project reference number ID17-0078.

NKS conveys its gratitude to all organizations and persons who by means of financial support or contributions in kind have made the work presented in this report possible.


## Disclaimer

The views expressed in this document remain the responsibility of the author(s) and do not necessarily reflect those of NKS. In particular, neither NKS nor any other organisation or body supporting NKS activities can be held responsible for the material presented in this report.

## References


Allison, C.M., Berna, G.A., Chambers, R., Coryell, E.W., Davis, K.L., Hagrman, D.L., Hagrman, D.T., Hampton, N.L., Hohorst, J.K., Mason, R.E., McComas, M.L., McNeil, K.A., Miller, R.L., Olsen, C.S., Reymann, G.A., Siefken, L.J., 1993. SCDAP/RELAP5/MOD3.1 Code Manual, Volume IV: MATPRO--A Library of Materials Properties for Light-Water-Reactor Accident Analysis.

Bunge, H.-J. 2013. Texture analysis in materials science: mathematical methods. Elsevier. 614 pp. ISBN: 0-408.10642-5.

Canon, R.F., Roberts, J.T.A., Beals, R.J., 1971. Deformation of $UO_2$ at High Temperatures. J. Am. Ceram. Soc. 54, 105–112. https://doi.org/https://doi.org/10.1111/j.1151-2916.1971.tb12230.x.

Chakraborty, P., Zhang, Y., Tonks, M.R., 2016. Multi-scale modeling of microstructure dependent intergranular brittle fracture using a quantitative phase-field based method. Comput. Mater. Sci. 113, 38–52. https://doi.org/10.1016/J.COMMATSCI.2015.11.010.

Costa, DR, Hedberg, M, Middleburgh, SC, Wallenius, J, Olsson, P & Lopes, DA. 2020. UN microspheres embedded in $UO_2$ matrix: an innovative accident tolerant fuel. Journal of Nuclear Materials. 540: 152355. DOI: https://doi.org/10.1016/j.jnucmat.2020.152355.

Costa, DR, Hedberg, M, Middleburgh, SC, Wallenius, J, Olsson, P & Lopes, DA. 2021. Oxidation of UN/$U_2N_3$-$UO_2$ composites: an evaluation of $UO_2$ as an oxidation barrier for the nitride phases. Journal of Nuclear Materials. 544: 152700. DOI: https://doi.org/10.1016/j.jnucmat.2020.152700.

German, R.M. 2014. Sintering: from empirical observations to scientific principles, first ed. Butterworth-Heinemann, Oxford. 544 pp. ISBN: 978-0-12-401682-8.

Hales, J.D., Gamble, K.A., Spencer, B.W., Novascone, S.R., Pastore, G., Liu, W., Stafford, D.S., Williamson, R.L., Perez, D.M., Gardner, R.J., Casagranda, A., Galloway, J., Matthews, C., Unal, C., Carlson, N., 2016a. INL/MIS-13-30307 Rev. 3 BISON Users Manual.

Hales, J.D., Williamson, R.L., Novascone, S.R., Pastore, G., Spencer, B.W., Gamble, K.A., Perez, D.M., Gardner, R.J., Liu, W., Galloway, J., Matthews, C., Unal, C., Carlson, N., 2016b. INL/EXT-13-29930 Rev. 3 BISON Theory Manual.

Hälldahl, L. 1985. Studies of reactions occurring in the AUC-process: from $UF_6$ to sintering $UO_2$ pellets. Doctoral thesis. Stockholm University, Sweden. ISBN 91-7146-647-9, Series: Chemical communications, 0366-5607;1985:2.

Igata, N., Domoto, K., 1973. Fracture stress and elastic modulus of uranium dioxide including excess oxygen. J. Nucl. Mater. 45, 317–322. https://doi.org/https://doi.org/10.1016/0022-3115(73)90165-7.

Iltis, X, Gey, N, Cagna, C, Hazotte, A & Sornay, Ph. 2015. Microstructural evolution of uranium dioxide following compression creep tests: an EBSD and image analysis study. Journal of Nuclear Materials. 456; 426-435. DOI: http://dx.doi.org/10.1016/j.jnucmat.2014.10.005.

Johnson, KD & Lopes, DA. 2018. Grain growth in uranium nitride prepared by spark plasma sintering, Journal of Nuclear Materials. 503: 75-80. DOI: https://doi.org/10.1016/j.jnucmat.2018.02.041.

Kramman, M.A., Freeburn, H.R., 1987. ESCORE--the EPRI steady-state core reload evaluator code: General description. EPRI NP-5100.

Lee, M-C & Wu, C-J. 1991. Conversion of $UF_6$ to $UO_2$: a quasi-optimization of the ammonium uranyl carbonate process. Journal of Nuclear Materials. 185: 190-201. DOI: https://doi.org/10.1016/0022-3115(91)90335-5.

Maslova, OA, Iltis, X, Desgranges, L, Ammar, MR, Genevois, C, de Bilbao, E, Canizarès, A, Barannikova, SA, Leontyev, IN & Simon, P. 2019. Characterization of an $UO_2$ ceramic via Raman imaging and electron backscattering diffraction. Materials Characterization. 147: 280-285. DOI: https://doi.org/10.1016/j.matchar.2018.11.006.

Nerikar, PV, Rudman, K, Desai, TG, Byler, D, Unal, C, McClellan, KJ, Phillpot, SR, Sinnott, SB, Peralta, P, Uberuaga, BP & Stanekw, CR. 2011. Grain boundaries in uranium dioxide: scanning electron microscopy experiments and atomistic simulations. Journal of the American Ceramic Society. 94: 1893-1900. DOI: http://doi.org/10.1111/j.1551-2916.2010.04295.x.

Nolze, G. 2015. Euler angles and crystal symmetry. Crystal Research & Technology. 50: 188 201. DOI: http://doi.org/10.1002/crat.201400427.

OECD, 2015. State-of-the-Art Report on Multi-scale Modelling of Nuclear Fuels.

Oguma, M., 1982. Microstructure Effects on Fracture Strength of $UO_2$ Fuel Pellets. J. Nucl. Sci. Technol. 19, 1005–1014. https://doi.org/10.3327/jnst.19.1005.

Portelette, L., Amodeo, J., Madec, R., Soulacroix, J., Helfer, T., Michel, B., 2018. Crystal viscoplastic modeling of UO2 single crystal. J. Nucl. Mater. 510, 635–643. https://doi.org/10.1016/j.jnucmat.2018.06.035.

Radford, K.C., 1979. Effect of fabrication parameters and microstructure on the mechanical strength of UO2 fuel pellets. J. Nucl. Mater. 84, 222–236. https://doi.org/https://doi.org/10.1016/0022-3115(79)90165-X.

Rashid, Y., Dunham, R., Montgomery, R., 2004. Fuel Analysis and Licensing Code: FALCON MOD01. EPRI 10113.

Rundle, RE, Wilson, AS, Baenziger, NC & McDonald, RA. 1948. The structures of the carbides, nitrides and oxides of uranium. Journal of the American Chemical Society. 70:99-105. DOI: https://doi.org/10.1021/ja01181a029.

Saada, MB, X. Iltis, N. Gey, B. Beausir, A. Miard, P. Garcia, N. Maloufi, Influence of strain conditions on the grain sub-structuration in crept uranium dioxide pellets, J. Nucl. Mat. 518 (2019) 265 – 273, DOI: https://doi.org/10.1016/j.jnucmat.2019.02.052.

Saada, MB, X. Iltis, N. Gey, A. Miard, P. Garcia, N. Maloufi, Influence of intra-granular void

distribution on the grain sub-structure of $UO_2$ pellets after high temperature compression tests, J. Nucl. Mat. 545 (2021) 152632, DOI: https://doi.org/10.1016/j.jnucmat.2020.152632.
Salvo, M., Sercombe, J., Helfer, T., Sornay, P., Désoyer, T., 2015. Experimental characterization and modeling of UO2 grain boundary cracking at high temperatures and high strain rates. J. Nucl. Mater. 460, 184–199. https://doi.org/10.1016/j.jnucmat.2015.02.018.
Schwartz, AJ, Kumar, M, Adams, BL & Field, DP. Electron Backscatter Diffraction in Materials Science, Springer Science & Business Media, New York, 2000, ISBN: 978-1-4757-3205-4 (eBook), DOI: http://doi.org/10.1007/978-1-4757-3205-4.
Tian, X., Ge, L., Yu, Y., Wang, Y., You, Z., Li, L., 2019. Atomistic simulation of fracture in UO2 under tensile loading. J. Alloys Compd. 803, 42–50. https://doi.org/10.1016/J.JALLCOM.2019.06.267.
Werner, P., Routbort, J.L., 1983. Effect of pore shape on the fracture of UO2 up to high strain rates. J. Nucl. Mater. 113, 118–121. https://doi.org/10.1016/0022-3115(83)90172-1.

| | |
|---|---|
| Title | Towards high-fidelity fuel pellet fracture modelling in current and new fuel designs |
| Author(s) | Janne Heikinheimo, Jussi Peltonen and Diogo Ribeiro Costa |
| Affiliation(s) | VTT Technical Research Centre of Finland Ltd and KTH Royal Institute of Technology, Sweden |
| ISBN | 978-87-7893-537-3 |
| Date | March 2021 |
| Project | NKS-R / POMMI (Contract: AFT/NKS-R(20)131/7) |
| No. of pages | 17 |
| No. of tables | 0 |
| No. of illustrations | 13 |
| No. of references | 30 |

Abstract
max. 2000 characters

Cracking of $UO_2$ clearly requires detailed understanding of local microscopic and macroscopic stresses. Also, the structural details and their effects on the microcracking should be known. To improve the fuel fracture modelling, we have started the work towards binding the structural features of the pellets with the crack behaviour modelling. The report shows measurements of a standard pellet with EBSD techniques and reviews macroscopic stress behaviour in 2D horizontal plane for differently sized pellets applying the BISON fuel performance code.

The SEM-EBSD results of a standard $UO_2$ pellet showed a dense microstructure with small and round pores in inter- and intra-granular locations, which are characteristic of such a fuel. There was no preferential crystallographic orientation in the sample.

The stress behaviour in the fuel pellets was modelled during different power-up ramp rates. The varying diameter of pellets did not show any particular differences in the stress behaviour, except for the maximum stress location due to reduced pellet-cladding gap. Introducing a macroscopic crack in the pellet caused localization of the stress and the smeared cracking model of the BISON code worked well.

Key words: SEM-EBSD, $UO_2$ structure, BISON fuel performance code, von Mises stress, cracking